INTERNATIONAL JOURNAL OF
NUMERICAL ANALYSIS AND MODELING, *SERIES B*
Volume 1, Number 1, Pages 41–57

MULTISCALE NUMERICAL ALGORITHM FOR 3-D MAXWELL'S EQUATIONS WITH MEMORY EFFECTS IN COMPOSITE MATERIALS

YA ZHANG, LIQUN CAO, WALTER ALLEGRETTO, AND YANPING LIN

Abstract. This paper discusses the multiscale method for the time-dependent Maxwell's equations with memory effects in composite materials. The main difficulty is that one cannot use the usual multiscale asymptotic method (cf. [25, 4]) to solve this problem, due to the complication of the memory terms. The key steps addressed in this paper are to transfer the original integro-differential equations to the stationary Maxwell's equations by using the Laplace transform, to employ the multiscale asymptotic method to solve the stationary Maxwell's equations, and then to obtain the computational solution of the original problem by employing a quadrature formula for computing the inverse Laplace transform. Numerical simulations are then carried out to validate the multiscale numerical algorithm in the present paper.

Key words. time-dependent Maxwell's equations, memory effects, multiscale asymptotic expansion, Laplace transform, composite materials.

1. Introduction

The classical macroscopic electromagnetic field is described by four vector-valued functions of position $x \in R^3$ and time $t \in R$ denoted by $\mathbf{E}$, $\mathbf{D}$, $\mathbf{H}$, $\mathbf{B}$. The fundamental field vectors $\mathbf{E}$, $\mathbf{H}$ are the electric and magnetic field intensities, respectively. The vector-valued functions $\mathbf{D}$, $\mathbf{B}$ denote the electric displacement and magnetic induction, respectively. The classical macroscopic Maxwell's equations are given by:

$$\begin{cases} \nabla \times \mathbf{E} + \dfrac{\partial \mathbf{B}}{\partial t} = 0, \\ \nabla \times \mathbf{H} - \dfrac{\partial \mathbf{D}}{\partial t} = \mathbf{J}, \\ \nabla \cdot \mathbf{D} = \rho, \\ \nabla \cdot \mathbf{B} = 0, \end{cases} \tag{1}$$

where $\rho(\mathbf{x}, t)$, $\mathbf{J}(\mathbf{x}, t)$ are the electric charge density and the source current density, respectively.

The general form of the constitutive laws are the following:

$$\mathbf{D} = \epsilon \mathbf{E} + \int_0^t \Big\{ \sigma^{\mathbf{E}}(\mathbf{x}) + \nu^{\mathbf{E}}(\mathbf{x}, t-\tau) \Big\} \mathbf{E}(\mathbf{x}, \tau) d\tau \tag{2}$$

$$\mathbf{B} = \mu \mathbf{H} + \int_0^t \Big\{ \sigma^{\mathbf{H}}(\mathbf{x}) + \nu^{\mathbf{H}}(\mathbf{x}, t-\tau) \Big\} \mathbf{H}(\mathbf{x}, \tau) d\tau, \tag{3}$$

where $\epsilon = (\epsilon_{ij})$ and $\mu = (\mu_{ij})$ are the electric permittivity and the magnetic permeability of the media, respectively; $\sigma^{\mathbf{E}} = (\sigma^{\mathbf{E}}_{ij})$, $\nu^{\mathbf{E}}(\mathbf{x}, t)$ are the electric conductivity

Received by the editors August 1, 2010 and, in revised form, August 30, 2010.
2000 *Mathematics Subject Classification.* 65F10, 78M05.
This work was supported by National Natural Science Foundation of China (grant #60971121, #90916027), National Basic Research Program of China (grant #2010CB832702), RGF of SAR Hong Kong, China (PolyU 5017/09P), and by NSERC (Canada).

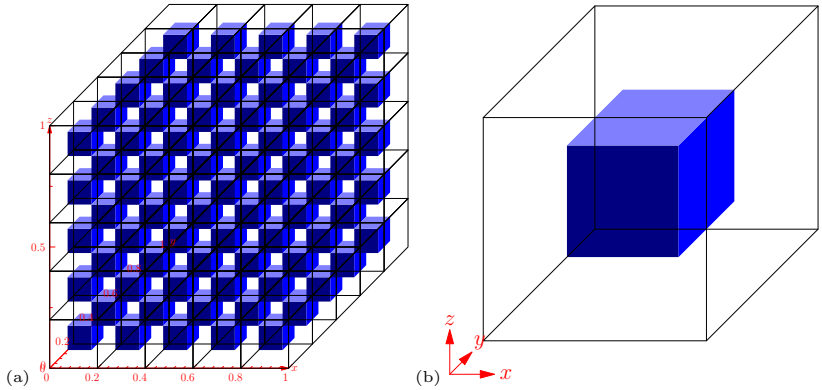

FIGURE 1. (a) Domain Ω; (b) the reference cell Q.

that characterizes the current density and the displacement susceptibility kernel function, respectively;
$\sigma^{\mathbf{H}} = (\sigma_{ij}^{\mathbf{H}})$, $\nu^{\mathbf{H}}(\mathbf{x},t)$ are the magnetic conductivity that characterizes the current density and the magnetic susceptibility, respectively. These are 3×3 positive-definite matrix-valued functions of position $x \in R^3$ in heterogeneous media. In the homogeneous case they are independent of x. In the isotropic case these parameters are scalars or diagonal matrices.

In this paper, we assume that $\sigma^H = \nu^H = 0$. From (1)-(3), by eliminating the magnetic field $\mathbf{H}$, we obtain

$$\begin{aligned}(4)\qquad &\epsilon(\mathbf{x})\frac{\partial^2\mathbf{E}(\mathbf{x},t)}{\partial t^2} + (\sigma^{\mathbf{E}}(\mathbf{x}) + \nu^{\mathbf{E}}(\mathbf{x},0))\frac{\partial \mathbf{E}(\mathbf{x},t)}{\partial t} + \nabla\times(\mu^{-1}(\mathbf{x})\nabla\times\mathbf{E})\\ &+\frac{\partial \nu^{\mathbf{E}}}{\partial t}(\mathbf{x},0)\mathbf{E}(\mathbf{x},t) + \int_0^t \frac{\partial^2\nu^{\mathbf{E}}(\mathbf{x},t-\tau)}{\partial t^2}\mathbf{E}(\mathbf{x},\tau)d\tau = -\frac{\partial}{\partial t}J(\mathbf{x},t),\end{aligned}$$

where $\mu^{-1}(\mathbf{x})$ denotes the inverse matrix of $\mu(\mathbf{x})$.

Suppose that $\Omega \subset R^3$ is a bounded polygonal convex domain or a smooth domain with a Lipschitz continuous boundary $\partial\Omega$ with a periodic microstructure as illustrated in Fig.1 (a) and (b). For convenience, we replace $\nabla\times\mathbf{u}$ with $\mathbf{curl}\,\mathbf{u}$. We then consider the following Maxwell's equations with rapidly oscillating coefficients:

$$(5)\qquad \begin{cases} B(\frac{\mathbf{x}}{\varepsilon})\frac{\partial^2\mathbf{E}^\varepsilon(\mathbf{x},t)}{\partial t^2} + C(\frac{\mathbf{x}}{\varepsilon})\frac{\partial\mathbf{E}^\varepsilon(\mathbf{x},t)}{\partial t} + G(\frac{\mathbf{x}}{\varepsilon})\mathbf{E}^\varepsilon(\mathbf{x},t) + \mathbf{curl}(A(\frac{\mathbf{x}}{\varepsilon})\mathbf{curl}\,\mathbf{E}^\varepsilon)\\ \quad + \int_0^t K(\frac{\mathbf{x}}{\varepsilon},t-\tau)\mathbf{E}^\varepsilon(\mathbf{x},\tau)d\tau = \mathbf{f}(\mathbf{x},t), \quad (\mathbf{x},t)\in\Omega\times(0,T)\\ \mathbf{E}^\varepsilon\times\mathbf{n} = 0, \quad (\mathbf{x},t)\in\partial\Omega\times(0,T)\\ \mathbf{E}^\varepsilon(\mathbf{x},0) = \mathbf{E}_0(\mathbf{x}), \quad \frac{\partial\mathbf{E}^\varepsilon(\mathbf{x},0)}{\partial t} = \mathbf{E}_1(\mathbf{x}),\end{cases}$$

Here ε denotes a small periodic parameter, which is the relative size of the unit cell. The matrix-valued functions $A(\frac{\mathbf{x}}{\varepsilon})$, $B(\frac{\mathbf{x}}{\varepsilon})$, $C(\frac{\mathbf{x}}{\varepsilon})$, $G(\frac{\mathbf{x}}{\varepsilon})$, $K(\frac{\mathbf{x}}{\varepsilon},t-\tau)$, and the vector-valued functions $\mathbf{f}(\mathbf{x},t)$, $\mathbf{E}_0(\mathbf{x})$, $\mathbf{E}_1(\mathbf{x})$ are known functions, $\mathbf{n} = (n_1,n_2,n_3)$ is the outward unit normal to $\partial\Omega$.

We first define the **curl** of a distribution $\mathbf{u} = (u_1,u_2,u_3)$ of $\mathcal{D}'(\Omega)^3$ by

$$\mathbf{curl}\ \mathbf{u} = (\frac{\partial u_3}{\partial x_2} - \frac{\partial u_2}{\partial x_3}, \frac{\partial u_1}{\partial x_3} - \frac{\partial u_3}{\partial x_1}, \frac{\partial u_2}{\partial x_1} - \frac{\partial u_1}{\partial x_2}).$$

Let the space $\mathbf{H}(\mathbf{curl};\Omega)$ be

$$\mathbf{H}(\mathbf{curl};\Omega)=\{\mathbf{u}\in(L^2(\Omega))^3;\mathbf{curl}\ \mathbf{u}\in(L^2(\Omega))^3\}$$

with the norm

$$\|\mathbf{u}\|_{\mathbf{H}(\mathbf{curl};\Omega)}=\{\|\mathbf{u}\|^2_{(L^2(\Omega))^3}+\|\mathbf{curl}\ \mathbf{u}\|^2_{(L^2(\Omega))^3}\}^{1/2},$$

and

$$\mathbf{H}_0(\mathbf{curl};\Omega)=closure\ of\ (C_0^\infty(\Omega))^3\ in\ \mathbf{H}(\mathbf{curl};\Omega),$$

or

$$\mathbf{H}_0(\mathbf{curl};\Omega)=\{\mathbf{u}\in\mathbf{H}(\mathbf{curl};\Omega);\mathbf{u}\times\mathbf{n}|_{\partial\Omega}=0\}.$$

Set $\mathcal{S}=\{(t,s)\in[0,T]^2;\ s\le t\}$ and $\mathcal{S}_D=\{(t,t);\ t\in[0,T]\}$. We introduce the following Sobolev spaces

$$\mathcal{W}^{1,p}(\mathcal{S};X)=\{\phi\in L^p(\mathcal{S};X);\ \frac{\partial\phi}{\partial t}\in L^p(\mathcal{S};X),\ \phi|_{\mathcal{S}_D}\in L^p(0,T;X)\},$$
$$\mathcal{W}^{2,p}(\mathcal{S};X)=\{\phi\in\mathcal{W}^{1,p}(\mathcal{S};X);\ \frac{\partial\phi}{\partial t}\in\mathcal{W}^{1,p}(\mathcal{S};X),\ \phi|_{\mathcal{S}_D}\in\mathcal{W}^{1,p}(0,T;X)\},$$

where X is a Banach space, the space $\mathcal{W}^{1,p}(\mathcal{S};X)$ and $\mathcal{W}^{2,p}(\mathcal{S};X)$ are respectively equipped with the norms

$$\|\phi\|_{1,p,X}=\|\frac{\partial\phi}{\partial t}\|_{L^p(\mathcal{S};X)}+\|\phi|_{\mathcal{S}_D}\|_{L^p(0,T;X)},$$
$$\|\phi\|_{2,p,X}=\|\frac{\partial\phi}{\partial t}\|_{1,p,X}+\|\phi|_{\mathcal{S}_D}\|_{\mathcal{W}^{1,p}(0,T;X)}.$$

We make the following assumptions:

($\mathbf{A_1}$) Let $\xi=\varepsilon^{-1}\mathbf{x}$, and assume that the elements of the matrices $A(\xi)$, $B(\xi)$, $C(\xi)$, $G(\xi)$, $K(\xi,t-\tau)$ are 1-periodic in ξ.

($\mathbf{A_2}$) The matrices $A(\xi)$ and $B(\xi)$ are symmetric and positive-definitive.

($\mathbf{A_3}$) A, B, C, $G\in L^\infty(\Omega;R^{3\times3})$, $K\in\mathcal{W}^{2,p}(\mathcal{S};L^\infty(\Omega;R^{3\times3}))$, and $\mathbf{f}\in\mathcal{W}^{1,1}(0,T;L^2(\Omega;R^3))$, $\mathbf{E}_0\in\mathbf{H}_0(\mathbf{curl};\Omega)$, $\mathbf{E}_1\in(L^2(\Omega))^3$.

Lemma 1.1 (see [3], Proposition 1) Under the assumptions of $(A_2)-(A_3)$, problem (5) has a unique solution $\mathbf{E}^\varepsilon\in\mathcal{W}^{1,\infty}(0,T;L^2(\Omega;R^3))\cap L^\infty(0,T;\mathbf{H}_0(\mathbf{curl};\Omega))$ that satisfies the following bounds:

$$\begin{aligned}&\|\mathbf{E}^\varepsilon\|_{L^\infty(0,T;\mathbf{H}_0(\mathbf{curl};\Omega))}+\|\partial_t\mathbf{E}^\varepsilon\|_{L^\infty(0,T;L^2(\Omega;R^3))}\\&\quad\le C\Big(\|\mathbf{f}\|_{\mathbf{H}_0(\mathbf{curl};\Omega)}+\|\mathbf{E}_0\|_{\mathbf{H}_0(\mathbf{curl};\Omega)}+\|\mathbf{E}_1\|_{L^2(\Omega))^3}\Big),\end{aligned}\tag{6}$$

where C is a constant independent of ε, $\partial_t\mathbf{E}^\varepsilon$ denotes the derivative of $\mathbf{E}^\varepsilon$ with respect to t.

Since problems (5) is an integro-differential equations with rapidly oscillating coefficients, a direct computation of (5) is extremely difficult, because it would require both a fine mesh and a lot of memory storage. Homogenization is a process in which the composite materials having a microscopic structure are replaced with an equivalent material having macroscopic properties. In this process of homogenization the rapidly oscillating coefficients are replaced by new effective constant coefficients. For the homogenization method of the Maxwell's equations in different media, there are a number of theoretical results, see [3, 11, 13, 23, 24]. Numerous numerical results have shown that the numerical accuracy of the homogenization method may not be satisfactory if ε is not sufficiently small. We can expect that the multiscale method for Maxwell's equations in composite materials is of crucial interest (see, e.g. [25, 3, 4, 5]). However, generally speaking, we can not directly use the classical multiscale asymptotic expansions to solve problem (5), due to

the emergence of the memory terms. Sheen et al.([21], [14], [15]) employ Laplace transforms to solve an integro-differential equation of parabolic type, and develop a numerical method for computing the inverse Laplace transform. In engineering applications, Tzou [22] also presents a quadrature formula for calculating the inverse Laplace transform. Numerous numerical results show Tzou's method remains competitive with other methods, see [22, 26].

This paper discusses the multiscale computation for problem (5) in specific case, see Section 2. The key steps addressed in the present paper are the application of the Laplace transform to convert problem (5) into stationary Maxwell's equations, to present the multiscale asymptotic expansion for the latter case, then to use the inverse Laplace transform to obtain the approximate solution of (5), where we employ Tzou's method for computing the inverse Laplace transform.

We organize this paper as follows. In Section 2, we develop the multiscale asymptotic expansion of the solution for the stationary Maxwell's equations by applying a Laplace transform to problem (5). Section 3 is devoted to the finite element computations for related problems and the multiscale finite element method for the stationary Maxwell's equations. In Section 4, we introduce the inverse Laplace transform and the Riemann-sum approximation, then obtain the multiscale approach for the original problem (5). Finally, numerical case studies are reported, and the simulations confirm the validity of the multiscale numerical algorithm presented in this paper.

Throughout the paper the Einstein summation convention on the repeated indices is adopted. By C we denote a positive constant independent of ε without distinction.

2. Stationary Maxwell's equations and the Multiscale Asymptotic Expansion

2.1. Stationary Maxwell's equations. To begin, we introduce the Laplace transform $\hat{g}(p) = \mathcal{L}(g) = \int_0^\infty g(t)e^{-pt}dt$ for any function $g \in L^1(0,\infty)$, $Re(p) > 0$, where $Re(p)$ denotes the real part of p. Thanks to Lemma 1.1, there exists a constant $p_0 > 0$ that depends only on the data such that the solution $\mathbf{E}^\varepsilon(\mathbf{x},t)$ to problem (5) has a Laplace transform for all $p \geq p_0 > 0$. Therefore, we apply the Laplace transform on both sides of (5) and obtain

(7)
$$\begin{cases} \Big(p^2 B(\frac{\mathbf{x}}{\varepsilon}) + pC(\frac{\mathbf{x}}{\varepsilon}) + G(\frac{\mathbf{x}}{\varepsilon}) + \widehat{K}(\frac{\mathbf{x}}{\varepsilon},p)\Big)\widehat{\mathbf{E}}^\varepsilon(\mathbf{x},p) + \mathbf{curl}\,(A(\frac{\mathbf{x}}{\varepsilon})\mathbf{curl}\,\widehat{\mathbf{E}}^\varepsilon(\mathbf{x},p)) \\ \quad = \hat{\mathbf{f}}(\mathbf{x},p) + (1+p)\mathbf{E}_0(\mathbf{x}) + \mathbf{E}_1(\mathbf{x}), \quad \mathbf{x} \in \Omega \\ \widehat{\mathbf{E}}^\varepsilon(\mathbf{x},p) \times \mathbf{n} = 0, \quad \mathbf{x} \in \partial\Omega, \quad p \geq p_0 > 0, \end{cases}$$

where $\hat{\mathbf{E}}^\varepsilon(\mathbf{x},p) = \mathcal{L}(\mathbf{E}^\varepsilon(\mathbf{x},t))$, $\hat{\mathbf{f}}(\mathbf{x},p) = \mathcal{L}(\mathbf{f}(\mathbf{x},t))$, $\widehat{K}(\frac{\mathbf{x}}{\varepsilon},p) = \mathcal{L}(K(\frac{\mathbf{x}}{\varepsilon},t))$.

Remark 2.1 Existence and uniqueness of the solution for problem (7) can be determined for any fixed $p \geq p_0 > 0$ based on Proposition 5 of [3]. Furthermore, we have
$\widehat{\mathbf{E}}^\varepsilon \in L^\infty(p_0,\infty;\mathbf{H}_0(\mathbf{curl};\Omega))$ and the uniform bounds

$$\|\widehat{\mathbf{E}}^\varepsilon(\mathbf{x},p)\|_{L^2(\Omega)} \leq \frac{C}{p}, \quad \|\mathbf{curl}\,\widehat{\mathbf{E}}^\varepsilon(\mathbf{x},p)\|_{L^2(\Omega)} \leq C, \quad \forall p \geq p_0 > 0,$$

where C is a constant independent of p.

2.2. Multiscale asymptotic expansion. In this section, we will study the multiscale asymptotic expansion of the solution to problem (7). We state that this is a

considerable challenge in general cases, in particular the determination of higher-order multiscale correctors. For more details, please refer to [3]. In this paper, we present the multiscale asymptotic expansion of the solution to problem (7) in the following specific case: B, C, G, K are independent of the space variable $\mathbf{x} \in \Omega$. For simplicity, let $B(\frac{\mathbf{x}}{\varepsilon}) = C(\frac{\mathbf{x}}{\varepsilon}) = G(\frac{\mathbf{x}}{\varepsilon}) \equiv I_3$, $\widehat{K}(\frac{\mathbf{x}}{\varepsilon}, p) \equiv \widehat{K}(p)$ without loss of generality, where I_3 is an 3×3 identity matrix. Under this assumption, problem (7) reduces to the following problem:

$$
\left\{
\begin{array}{l}
\mathbf{curl}\,(A(\dfrac{\mathbf{x}}{\varepsilon})\mathbf{curl}\,\widehat{\mathbf{E}}^{\varepsilon}(\mathbf{x},p)) + (p^2+p+1+\widehat{K}(p))\widehat{\mathbf{E}}^{\varepsilon}(\mathbf{x},p) \\
\quad = \hat{\mathbf{f}}(\mathbf{x},p) + (1+p)\mathbf{E}_0(\mathbf{x}) + \mathbf{E}_1(\mathbf{x}), \quad \mathbf{x} \in \Omega \\
\widehat{\mathbf{E}}^{\varepsilon}(\mathbf{x},p) \times \mathbf{n} = 0, \quad \mathbf{x} \in \partial\Omega, \quad p \geq p_0 > 0,
\end{array}
\right. \tag{8}
$$

Following the idea of [4], we define the multiscale asymptotic expansions to problem (8) as follows:

$$
\begin{array}{l}
\widehat{\mathbf{E}}^{\varepsilon,1}(\mathbf{x},p) = \widehat{\mathbf{E}}^{0}(\mathbf{x},p) + \varepsilon\Theta_1(\xi)\mathbf{curl}\,\widehat{\mathbf{E}}^{0}(\mathbf{x},p), \\
\widehat{\mathbf{E}}^{\varepsilon,2}(\mathbf{x},p) = \widehat{\mathbf{E}}^{0}(\mathbf{x},p) + \varepsilon\Theta_1(\xi)\mathbf{curl}\,\widehat{\mathbf{E}}^{0}(\mathbf{x},p) + \varepsilon^2\Theta_2(\xi)\mathbf{curl}^2\,\widehat{\mathbf{E}}^{0}(\mathbf{x},p),
\end{array} \tag{9}
$$

where $\mathbf{curl}^2 = \mathbf{curl}\,\mathbf{curl}$. We define

$$
\left\{
\begin{array}{l}
\mathbf{curl}_{\xi}\Big(A(\xi)\mathbf{curl}_{\xi}\Theta_1^q(\xi)\Big) = -\mathbf{curl}_{\xi}\Big(A(\xi)\mathbf{e}_q\Big), \quad \xi \in Q \\
\nabla_{\xi}\cdot\Theta_1^q(\xi) = 0, \quad \xi \in Q \\
\Theta_1^q(\xi) \times \nu = 0, \quad \xi \in \partial Q, \quad q = 1,2,3,
\end{array}
\right. \tag{10}
$$

where $\mathbf{e}_1 = \{1,0,0\}^T, \mathbf{e}_2 = \{0,1,0\}^T, \mathbf{e}_3 = \{0,0,1\}^T$ and $\mathbf{a}^T$ denotes the transpose of $\mathbf{a}$. We define the matrix-valued cell functions $\Theta_1(\xi) = (\Theta_1^1(\xi), \Theta_1^2(\xi), \Theta_1^3(\xi))$.

Let $\Xi_q(\xi) = -A(\xi)\mathbf{curl}_{\xi}\,\Theta_1^q(\xi) - A(\xi)\mathbf{e}_q + \hat{A}\mathbf{e}_q$, and define the scalar functions $\zeta^q(\xi)$, $q = 1,2,3$ as follows:

$$
\left\{
\begin{array}{l}
-\Delta_{\xi}\zeta^q(\xi) = div_{\xi}\,\Xi_q(\xi), \quad \xi \in Q, \\
\zeta^q(\xi) = 0, \quad \xi \in \partial Q, \quad q = 1,2,3,
\end{array}
\right. \tag{11}
$$

where div_{ξ} denotes the divergence operator with respect to ξ.

Given $div_{\xi}(\Xi_q(\xi) + \nabla_{\xi}\zeta^q(\xi)) = 0$, then we define

$$
\left\{
\begin{array}{l}
\mathbf{curl}_{\xi}\Big(A(\xi)\mathbf{curl}_{\xi}\Theta_2^q(\xi)\Big) = -\mathbf{curl}_{\xi}\Big(A(\xi)\Theta_1^q(\xi)\Big) \\
\quad -A(\xi)\mathbf{curl}_{\xi}\Theta_1^q(\xi) - A(\xi)\mathbf{e}_q + \hat{A}\mathbf{e}_q + \nabla\zeta^q, \quad \xi \in Q \\
\nabla_{\xi}\cdot\Theta_2^q(\xi) = 0, \quad \xi \in Q \\
\Theta_2^q(\xi) \times \nu = 0, \quad \xi \in \partial Q, \quad q = 1,2,3,
\end{array}
\right. \tag{12}
$$

where the homogenized coefficients matrix $\widehat{A}$ is computed by

$$
\widehat{A} = \int_Q \Big(A(\xi) + A(\xi)\,\mathbf{curl}_{\xi}\,\Theta_1(\xi)\Big)d\xi, \quad Q = (0,1)^3. \tag{13}
$$

We next define the matrix-valued cell functions $\Theta_2(\xi) = (\Theta_2^1(\xi), \Theta_2^2(\xi), \Theta_2^3(\xi))$.

Remark 2.2 Existence and uniqueness of the cell functions $\Theta_1^q(\xi)$, $\Theta_2^q(\xi)$, $q = 1,2,3$ can be established. For more details, please refer to [4].

Following the approach of [2, 4], we obtain the homogenized Maxwell's equations associated with problem (8) as follows:

$$\begin{cases} \mathbf{curl}\,(\widehat{A}\,\mathbf{curl}\,\widehat{\mathbf{E}}^0(\mathbf{x},p)) + (p^2+p+1+\widehat{K}(p))\widehat{\mathbf{E}}^0(\mathbf{x},p) \\ \quad = \hat{\mathbf{f}}(\mathbf{x},p) + (1+p)\mathbf{E}_0(\mathbf{x}) + \mathbf{E}_1(\mathbf{x}), \quad \mathbf{x}\in\Omega \\ \widehat{\mathbf{E}}^0(\mathbf{x},p)\times\mathbf{n} = 0, \quad \mathbf{x}\in\partial\Omega, \end{cases} \tag{14}$$

where $\mathbf{n} = (n_1, n_2, n_3)$ is the outward unit normal to $\partial\Omega$.

Remark 2.3 It can be proved that the homogenized coefficients matrix $\widehat{A}$ is symmetric and positive-definite. Existence and uniqueness of the solution to problem (14) can be established on the basis of Proposition 5 of [3], for any fixed $p \geq p_0 > 0$.

3. The Edge Finite Element Computations for Related Problems

3.1. The adaptive edge finite element method for computing cell functions $\Theta_1^q(\xi)$,

$\Theta_2^q(\xi)\, q = 1, 2, 3$**.** The variational problem of (10) is to find $\Theta_1^q(\xi) \in \mathbf{H}_0(\mathbf{curl}; Q)$ such that

$$b(\Theta_1^q, \mathbf{v}) = -\int_Q A(\xi)\mathbf{e}_q \cdot \mathbf{curl}_\xi \mathbf{v}(\xi)d\xi, \quad \forall \mathbf{v}\in \mathbf{H}_0(\mathbf{curl}; Q), \quad q = 1, 2, 3, \tag{15}$$

where we set the bilinear form

$$b(\mathbf{u}, \mathbf{v}) = \int_Q A(\xi)\mathbf{curl}_\xi \mathbf{u}(\xi) \cdot \mathbf{curl}_\xi \mathbf{v}(\xi)d\xi, \tag{16}$$

the scalar product $\mathbf{u}\cdot\mathbf{v} = u_i v_i$ and the reference cell $Q = (0, 1)^3$.

We employ an adaptive multilevel method presented in [7]. In solving (11) and (12), we apply the same mesh as (10). We introduce some notation: Let $\mathcal{T}_k$ be a sequence of tetrahedrons of the reference cell Q and $\mathcal{F}_k$ be the set of faces not lying on ∂Q , $k \geq 0$. The finite element space U_k over $\mathcal{T}_k$ is defined by

$$\begin{aligned} U_k = \{\mathbf{v}\in \mathbf{H}(\mathbf{curl}; Q): \quad & \mathbf{v}\times\nu|_{\partial Q} = 0 \quad \text{and} \\ & \mathbf{v}|_T = \mathbf{a}_T + \mathbf{b}_T \times \mathbf{x} \quad \text{with} \quad \mathbf{a}_T, \mathbf{b}_T \in R^3, \quad \forall T\in\mathcal{T}_k\}. \end{aligned}$$

Degrees of freedom on every $T \in \mathcal{T}_k$ are $\int_{E_i} \mathbf{v}\cdot d\mathbf{l}$, $i = 1, \cdots, 6$, where $E_1, \cdots, E_6$ are the six edges of T. For any $T \in \mathcal{T}_k$ and $F \in \mathcal{F}_k$, we denote the diameters of T and F by h_T and h_F, respectively.

Let $\Theta_{1,k}^q$, $q = 1, 2, 3$ denote the finite element approximate solutions of Θ_1^q, $q = 1, 2, 3$ in the finite element space U_k, respectively. Then,

$$b(\Theta_{1,k}^q, \mathbf{v}_k) = -\int_Q A(\xi)\mathbf{e}_q \cdot \mathbf{curl}_\xi \mathbf{v}_k(\xi)d\xi, \quad \forall \mathbf{v}_k \in U_k, \quad q = 1, 2, 3. \tag{17}$$

Following Theorems 3.3 and 3.4 of [7], we give *a posteriori* error estimates for Θ_1^q, $q = 1, 2, 3$, as follows:

$$\|\Theta_1^q(\xi) - \Theta_{1,k}^q(\xi)\|^2_{\mathbf{H}_0(\mathbf{curl};Q)} \leq C\Big(\sum_{T\in\mathcal{T}_k} \eta_T^2 + \sum_{F\in\mathcal{F}_k} \eta_F^2\Big), \tag{18}$$

where

$$\begin{aligned} \eta_T^2 &= h_T^2 \|\mathbf{curl}_\xi\, A(\xi)\mathbf{e}_q + \mathbf{curl}_\xi\Big(A(\xi)\mathbf{curl}_\xi\, \Theta_{1,k}^q(\xi)\Big)\|^2_{0,T} \\ \eta_F^2 &= h_F \|[A(\xi)\mathbf{curl}_\xi\, \Theta_{1,k}^q(\xi)\times\nu]|_F\|^2_{0,F}. \end{aligned}$$

In order to compute $\zeta^q(\xi)$ and $\Theta_2^q(\xi)$, we need to solve problems (11) and (12) numerically. Define a linear finite element space over $\mathcal{T}_k$ given by

$$S_k^0(Q) = \{w_k \in C^0(\overline{Q}): \quad w_k|_T \in P_1,\, T\in\mathcal{T}_k,\, w_k|_{\partial Q} = 0\} \subset H_0^1(Q), \tag{19}$$

where P_1 is the set of all piecewise linear polynomials.

The discrete variational problem of (11) is to find: $\zeta_k^q \in S_k^0(Q)$ such that

$$\int_Q \nabla_\xi \zeta_k^q \cdot \nabla_\xi w_k d\xi = \int_Q \Xi_q(\xi) \cdot \nabla_\xi w_k d\xi, \quad \forall w_k \in S_k^0(Q), \quad q = 1, 2, 3, \tag{20}$$

where $\Xi_q(\xi)$ is given in (11).

A weak solution of the cell problem (12) is to find $\Theta_2^q(\xi) \in \mathbf{H}_0(\mathbf{curl}; Q)$ such that

$$\begin{array}{l} b(\Theta_2^q, \mathbf{v}) = -\int_Q A(\xi)\Theta_1^q(\xi) \cdot \mathbf{curl}_\xi \mathbf{v} d\xi + \int_Q \Xi_q(\xi) \cdot \mathbf{v} d\xi \\ \quad -\int_Q \nabla_\xi \zeta^q(\xi) \cdot \mathbf{v} d\xi, \quad \forall \mathbf{v} \in \mathbf{H}_0(\mathbf{curl}; Q), \quad q = 1, 2, 3, \end{array} \tag{21}$$

where the bilinear form $b(\mathbf{u}, \mathbf{v})$ is defined in (16), $\Theta_1^q(\xi)$, $q = 1, 2, 3$ are given in (10).

The discrete variational problem of (12) is to find $\Theta_{2,k}^q \in U_k$ such that

$$\begin{array}{l} b(\Theta_{2,k}^q, \mathbf{v}_k) = -\int_Q A(\xi)\Theta_{1,k}^q(\xi) \cdot \mathbf{curl}_\xi \mathbf{v}_k d\xi + \int_Q \Xi_q^k(\xi) \cdot \mathbf{v}_k d\xi \\ \quad -\int_Q \nabla_\xi \zeta_k^q(\xi) \cdot \mathbf{v}_k d\xi, \quad \forall \mathbf{v}_k \in U_k, \quad q = 1, 2, 3, \end{array} \tag{22}$$

where

$$\Xi_q^k(\xi) = -A(\xi)\mathbf{curl}_\xi \Theta_{1,k}^q(\xi) - A(\xi)\mathbf{e}_q + \hat{A}^k \mathbf{e}_q,$$

$$\widehat{A}^k = \int_Q [A(\xi) + A(\xi)\,\mathbf{curl}_\xi\, \Theta_{1,k}(\xi)] d\xi,$$

and

$$\Theta_{1,k}(\xi) = (\Theta_{1,k}^1(\xi), \Theta_{1,k}^2(\xi), \Theta_{1,k}^3(\xi)).$$

3.2. The edge finite element method for solving the homogenized Maxwell's equations. We recall (13), (14) and (17). In practice, we need to solve the following modified homogenized Maxwell's equations:

$$\left\{ \begin{array}{l} \mathbf{curl}\,(\widehat{A}^{h_0}\,\mathbf{curl}\,\widehat{\tilde{\mathbf{E}}}^0(\mathbf{x}, p)) + (p^2 + p + 1 + \widehat{K}(p))\widehat{\tilde{\mathbf{E}}}^0(\mathbf{x}, p) \\ \quad = \hat{\mathbf{f}}(\mathbf{x}, p) + (1 + p)\mathbf{E}_0(\mathbf{x}) + \mathbf{E}_1(\mathbf{x}), \quad \mathbf{x} \in \Omega \\ \widehat{\tilde{\mathbf{E}}}^0(\mathbf{x}, p) \times \mathbf{n} = 0, \quad \mathbf{x} \in \partial\Omega, \end{array} \right. \tag{23}$$

where

$$\widehat{A}^{h_0} = \int_Q [A(\xi) + A(\xi)\,\mathbf{curl}_\xi\, \Theta_{1,h_0}(\xi)] d\xi,$$

$\Theta_{1,h_0}(\xi)$ denotes the finite element solution of $\Theta_1(\xi)$ and h_0 is the final mesh parameter of the adaptive finite element method for computing $\Theta_1(\xi)$.

In this section, we discuss the finite element computation for the homogenized Maxwell's equations (23) in a whole domain Ω. Let $\mathcal{T}^h = \{e\}$ be a regular family of tetrahedrons of Ω and $h = \max_e\{h_e\}$. We define the finite element space of $\mathbf{H}_0(\mathbf{curl}; \Omega)$ consisting of the linear edge elements by

$$X_h(\Omega) = \{\mathbf{v}_h \in \mathbf{H}(\mathbf{curl}; \Omega) : \quad \mathbf{v}_h|_e \in R_1,\ \mathbf{v}_h \times \mathbf{n} = 0 \text{ on } \partial\Omega\}, \tag{24}$$

where $\mathbf{n}$ is the outward unit normal to the boundary $\partial\Omega$ and R_1 is defined in (5.32) of ([16], p.128).

The discrete variational form of problem (23) is the following:

$$\left\{ \begin{array}{l} a(\widehat{\tilde{\mathbf{E}}}_h^0, v_h) + (p^2 + p + 1 + \widehat{K}(p))(\widehat{\tilde{\mathbf{E}}}_h^0, v_h) \\ \quad = (\hat{\mathbf{f}} + (1 + p)\mathbf{E}_0 + \mathbf{E}_1, \mathbf{v}_h), \quad \forall \mathbf{v}_h \in X_h(\Omega), \end{array} \right. \tag{25}$$

where

$$a(\mathbf{u},\mathbf{v}) = \int_\Omega \widehat{A}^{h_0}\mathbf{curl}\,\mathbf{u}\cdot\mathbf{curl}\,\mathbf{v}d\mathbf{x}. \tag{26}$$

Set $P = p^2+p+1+\widehat{K}(p) = \alpha+i\beta$ and $\mathbf{F} = \hat{\mathbf{f}}+(1+p)\mathbf{E}_0+\mathbf{E}_1 = \mathbf{f}_1+i\mathbf{f}_2$, where $i=\sqrt{-1}$. Let $\{\phi_j(\mathbf{x})\}_{j=1}^N$ be a set of basis of $X_h(\Omega)$ and $\widehat{\tilde{\mathbf{E}}}_h^0(\mathbf{x},p) = \sum\limits_{j=1}^N \chi_j\varphi_j(\mathbf{x})$. Then the discrete system (25) is equivalent to

$$\sum_{j=1}^N a(\varphi_j,\varphi_k)\chi_j + \sum_{j=1}^N P(\varphi_j,\varphi_k)\chi_j = (\mathbf{F},\varphi_k),\ k=1,2,\ldots,N. \tag{27}$$

We denote by $\hat{K}_h := (a(\varphi_j,\varphi_k))_{jk}$ the stiffness matrix, $M_h := ((\varphi_j,\varphi_k))_{jk}$ the mass matrix, $\chi_j = u_j+iv_j$, $u=(u_1,\cdots,u_N)^T$, $v=(v_1,\cdots,v_N)^T$, $F_1 = ((\mathbf{f}_1,\varphi_1),(\mathbf{f}_1,\varphi_2),\cdots,(\mathbf{f}_1,\varphi_N))^T$, $F_2 = ((\mathbf{f}_2,\varphi_1),\cdots,(\mathbf{f}_2,\varphi_N))^T$. Therefore, we solve the linear system as follows:

$$\begin{pmatrix} \hat{K}_h+\alpha M_h & -\beta M_h \\ \beta M_h & \hat{K}_h+\alpha M_h \end{pmatrix}\begin{pmatrix} u \\ v \end{pmatrix} = \begin{pmatrix} F_1 \\ F_2 \end{pmatrix}. \tag{28}$$

3.3. The multiscale finite element method for the stationary Maxwell's equations. The multiscale numerical algorithm for the stationary Maxwell's equations consists of the following steps:

Step 1: Compute the cell functions $\Theta_1(\xi)$ and $\Theta_2(\xi)$ defined in (10) and (12) in the reference cell Q.

Step 2: Solve the modified homogenized stationary Maxwell's equations (23) in the whole domain Ω in a coarse mesh for any fixed $p \ge p_0 > 0$.

Step 3: Define the first-order and the second-order difference quotients, then replace $\mathbf{curl}\,\widehat{\tilde{\mathbf{E}}}^0(\mathbf{x},p)$, $\mathbf{curl}^2\,\widehat{\tilde{\mathbf{E}}}^0(\mathbf{x},p)$ by them, where $\widehat{\tilde{\mathbf{E}}}^0(\mathbf{x},p)$ is the solution of the modified homogenized stationary Maxwell's equations (23).

Define the first-order **curl** difference quotients given by

$$\delta_c\widehat{\tilde{\mathbf{E}}}_h^0(N_m,p) = \frac{1}{\tau(N_m)}\sum_{e\in\sigma(N_m)}\mathbf{curl}\,\widehat{\tilde{\mathbf{E}}}_h^0|_e(N_m,p), \tag{29}$$

where $\sigma(N_m)$ is the set of elements with node N_m, $\tau(N_m)$ is the number of elements of $\sigma(N_m)$, $\mathbf{curl}\,\widehat{\tilde{\mathbf{E}}}_h^0(N_m,p)$ is the value of the $\mathbf{curl}\,\widehat{\tilde{\mathbf{E}}}_h^0$ at node N_m associated with element e.

The second-order difference quotients are given as follows:

$$\delta_c^2\widehat{\tilde{\mathbf{E}}}_h^0(N_m,p) = \frac{1}{\tau(N_m)}\sum_{e\in\sigma(N_m)}\sum_{j=1}^d \delta_c\widehat{\tilde{\mathbf{E}}}_h^0(P_j,p)\mathbf{curl}\,\psi_j|_e(N_m), \tag{30}$$

where d is the number of nodes on e; P_j, $j=1,\cdots,d$ are the nodes of e and ψ_j, $j=1,\cdots,d$ are the Lagrange's shape functions.

Define the multiscale numerical algorithm for the stationary Maxwell's equations as follows

$$\begin{aligned} \widehat{\mathbf{E}}_{h_0,h}^{\varepsilon,1}(\mathbf{x},p) &= \widehat{\tilde{\mathbf{E}}}_h^0(\mathbf{x},p)+\varepsilon\Theta_{1,h_0}(\xi)\delta_c\widehat{\tilde{\mathbf{E}}}_h^0(\mathbf{x},p), \\ \widehat{\mathbf{E}}_{h_0,h}^{\varepsilon,2}(\mathbf{x},p) &= \widehat{\tilde{\mathbf{E}}}_h^0(\mathbf{x},p)+\varepsilon\Theta_{1,h_0}(\xi)\delta_c\widehat{\tilde{\mathbf{E}}}_h^0(\mathbf{x},p)+\varepsilon^2\Theta_{2,h_0}(\xi)\delta_c^2\widehat{\tilde{\mathbf{E}}}_h^0(\mathbf{x},p), \end{aligned} \tag{31}$$

where $\widehat{\tilde{\mathbf{E}}}_h^0(\mathbf{x},p)$ is the finite element solution of $\widehat{\tilde{\mathbf{E}}}^0(\mathbf{x},p)$; $\Theta_{1,h_0}(\xi)$, $\Theta_{2,h_0}(\xi)$ are respectively the finite element solutions of $\Theta_1(\xi)$, $\Theta_2(\xi)$; $\delta_c\widehat{\tilde{\mathbf{E}}}_h^0(\mathbf{x},p)$, $\delta_c^2\widehat{\tilde{\mathbf{E}}}_h^0(\mathbf{x},p)$ denote the interpolation functions of $\delta_c\widehat{\tilde{\mathbf{E}}}_h^0(N_m,p)$, $\delta_c^2\widehat{\tilde{\mathbf{E}}}_h^0(N_m,p)$, respectively.

4. The Inverse Laplace Transform and the Approximate Solution for the Original Problem

4.1. The inverse Laplace transform. Define the inverse Laplace transform of a function $\hat{\mathbf{u}}(\mathbf{x},p)$ as follows:

$$\mathbf{u}(\mathbf{x},t)=\mathcal{L}^{-1}(\hat{\mathbf{u}}(\mathbf{x},p))=\frac{1}{2\pi i}\int_{\gamma-i\infty}^{\gamma+i\infty}\hat{\mathbf{u}}(\mathbf{x},p)e^{pt}dp, \tag{32}$$

where $p=\gamma+i\varsigma$, $Re(p)>0$, where $Re(p)$ denotes the real part of p.

To compute the inverse Laplace transform (32), we introduce the Riemann-sum approximation (see [22])

$$\mathbf{u}(\mathbf{x},t)=\frac{e^{\gamma t}}{t}[\frac{1}{2}\hat{\mathbf{u}}(\mathbf{x},\gamma)+Re\sum_{k=1}^{\infty}\hat{\mathbf{u}}(\mathbf{x},\gamma+\frac{ik\pi}{t})(-1)^k], \tag{33}$$

where $\gamma=\dfrac{4.7}{t}$.

In practice, we define the truncated function for the Riemann-sum approximation as follows:

$$\mathbf{u}_M(\mathbf{x},t)=\frac{e^{\gamma t}}{t}\Big\{\frac{1}{2}\hat{\mathbf{u}}(\mathbf{x},\gamma)+Re\sum_{k=1}^{M}\hat{\mathbf{u}}(\mathbf{x},\gamma+\frac{ik\pi}{t})(-1)^k\Big\}. \tag{34}$$

4.2. The multiscale approach for the original problem (5). Once we obtain the numerical solutions $\widehat{\tilde{\mathbf{E}}}_h^0(\mathbf{x},p)$, $\widehat{\mathbf{E}}_{h_0,h}^{\varepsilon,s}(\mathbf{x},p)$, $s=1,2$, we can apply the inverse Laplace transform to get the approximate solution of the original problem (5). For any fixed time $t=t^*$, we simultaneously solve a set of the homogenized Maxwell's equations (23) with complex coefficients in a coarse mesh for different p_k, which are independent and may therefore be done in parallel. Here we choose $p_k=\dfrac{4.7}{t^*}+i\dfrac{k\pi}{t^*}$, $k=0,1,2,\cdots,M$.

Thanks to (31) and (34), we get the multiscale approximate solutions for the original problem (5) as follows:

$$\mathbf{E}_{M,h_0,h}^0(\mathbf{x},t^*) = \frac{e^{\gamma t^*}}{t^*}\{\frac{1}{2}\widehat{\tilde{\mathbf{E}}}_h^0(\mathbf{x},p_0)+Re\sum_{k=1}^{M}\widehat{\tilde{\mathbf{E}}}_h^0(\mathbf{x},p_k)\}, \tag{35}$$

$$\begin{aligned}\mathbf{E}_{M,h_0,h}^{\varepsilon,1}(\mathbf{x},t^*) &= \frac{e^{\gamma t^*}}{t^*}\{\frac{1}{2}[\widehat{\tilde{\mathbf{E}}}_h^0(\mathbf{x},p_0)+\varepsilon\Theta_{1,h_0}(\xi)\delta_c\widehat{\mathbf{E}}_h^0(\mathbf{x},p_0)]\\ &+ Re\sum_{k=1}^{M}[\widehat{\tilde{\mathbf{E}}}_h^0(\mathbf{x},p_k)+\varepsilon\Theta_{1,h_0}(\xi)\delta_c\widehat{\tilde{\mathbf{E}}}_h^0(\mathbf{x},p_k)](-1)^k\}\end{aligned} \tag{36}$$

$$\begin{aligned}\mathbf{E}_{M,h_0,h}^{\varepsilon,2}(\mathbf{x},t^*) &= \frac{e^{\gamma t^*}}{t^*}\{\frac{1}{2}[\widehat{\tilde{\mathbf{E}}}_h^0(\mathbf{x},p_0)+\varepsilon\Theta_{1,h_0}(\xi)\delta_c\widehat{\tilde{\mathbf{E}}}_h^0(\mathbf{x},p_0)+\varepsilon^2\Theta_{2,h_0}(\xi)\delta_c^2\widehat{\tilde{\mathbf{E}}}_h^0(\mathbf{x},p_0)]\\ &+Re\sum_{k=1}^{M}[\widehat{\tilde{\mathbf{E}}}_h^0(\mathbf{x},p_k)+\varepsilon\Theta_{1,h_0}(\xi)\delta_c\widehat{\tilde{\mathbf{E}}}_h^0(\mathbf{x},p_k)+\varepsilon^2\Theta_{2,h_0}(\xi)\delta_c^2\widehat{\tilde{\mathbf{E}}}_h^0(\mathbf{x},p_k)](-1)^k\},\end{aligned} \tag{37}$$

where $\widehat{\widetilde{\mathbf{E}}}_h^0(\mathbf{x}, p_k)$, $k = 0, 1, \cdots, M$ are the finite element solutions of problem (23) for different p_k, $k = 0, 1, \cdots, M$. The matrix-valued functions $\Theta_{1,h_0}(\xi) = (\Theta^1_{1,h_0}(\xi), \Theta^2_{1,h_0}(\xi), \Theta^3_{1,h_0}(\xi))$, $\Theta_{2,h_0}(\xi) = (\Theta^1_{2,h_0}(\xi), \Theta^2_{2,h_0}(\xi), \Theta^3_{2,h_0}(\xi))$, where $\Theta^q_{1,h_0}(\xi)$, $\Theta^q_{2,h_0}(\xi)$, $q = 1, 2, 3$ are the finite element solutions of cell problems (10) and (12). $\delta_c \widehat{\widetilde{\mathbf{E}}}_h^0(\mathbf{x}, p_k)$, $\delta_c^2 \widehat{\widetilde{\mathbf{E}}}_h^0(\mathbf{x}, p_k)$ are given in (29) and (30), respectively. h_0, h are respectively the mesh parameters of the reference cell Q and the whole domain Ω.

5. Numerical Case Studies

To validate the developed multiscale algorithm, we present numerical simulations for the following case studies. We consider the following 3-D time-dependent Maxwell's equations in composite materials with memory effects as follows:

$$
\begin{cases}
\dfrac{\partial^2 \mathbf{E}^\varepsilon}{\partial t^2} + \dfrac{\partial \mathbf{E}^\varepsilon}{\partial t} + \mathbf{E}^\varepsilon + \mathbf{curl}\,(A(\dfrac{\mathbf{x}}{\varepsilon})\mathbf{curl}\,\mathbf{E}^\varepsilon) \\
\quad + \displaystyle\int_0^t K(t-\tau)\mathbf{E}^\varepsilon(\mathbf{x},\tau)d\tau = \mathbf{f}(\mathbf{x},t), \quad (\mathbf{x},t) \in \Omega \times (0,T) \\
\mathbf{E}^\varepsilon \times \mathbf{n} = 0, \quad (\mathbf{x},t) \in \partial\Omega \times (0,T) \\
\mathbf{E}^\varepsilon(\mathbf{x},0) = \mathbf{E}_0(\mathbf{x}), \quad \dfrac{\partial \mathbf{E}^\varepsilon}{\partial t}(\mathbf{x},0) = \mathbf{E}_1(\mathbf{x}),
\end{cases} \tag{38}
$$

Example 5.1 We consider problem (38) and assume that a whole domain Ω and the reference cell $Q = (0,1)^3$ are shown as in Fig.1: (a) and (b). Let $\varepsilon = \frac{1}{5}$, $T = 0.5$, $K(t) = e^{-t}$. Two cases are considered in our numerical simulations, and let a_{ij1} denote the value of a_{ij} in the inside cube of Q, and a_{ij0} denote the value of a_{ij} in the other part of Q.

Case 5.1: $a_{ij0} = 100\delta_{ij}$, $a_{ij1} = \delta_{ij}$; $\mathbf{f} = (500t, 500t, 500t)^T$.

Case 5.2: $a_{ij0} = 1000\delta_{ij}$, $a_{ij1} = \delta_{ij}$; $\mathbf{f} = (5000t, 5000t, 5000t)^T$,

where δ_{ij} is a Kronecker symbol, and $\mathbf{a}^T$ denotes the transpose of $\mathbf{a}$.

To show the numerical accuracy of the present method, we need to know the exact solution of problem (38). However, since it is extremely difficult to find out the exact solution of (38), we replace $\mathbf{E}^\varepsilon(\mathbf{x}, t)$ by the numerical solution in a fine mesh. In a standard approach, we first apply the linear edge element method to get the semi-discrete system for problem (38), and then employ the backward Euler scheme to solve the system and the memory term (see [6]). We take the time step $\Delta t = 0.005$. Without confusion, $\mathbf{E}^\varepsilon(\mathbf{x}, t)$ denotes the numerical solution of the original problem (38) in a fine mesh. It should be emphasized that this step is not necessary in real applications.

We recall that the key steps of the method presented in this paper are to apply the Laplace transform to convert problem (38) into the stationary problem (23), to use the multiscale numerical algorithm (31) to solve problem (23), then to employ the numerical formulas (35)-(37) for computing the inverse Laplace transform to get the approximate solutions of the original problem (38). It should be remembered that $\mathbf{E}^0_{M,h_0,h}(\mathbf{x}, t)$, $\mathbf{E}^{\varepsilon,1}_{M,h_0,h}(\mathbf{x}, t)$, $\mathbf{E}^{\varepsilon,2}_{M,h_0,h}(\mathbf{x}, t)$ denote the homogenized numerical solution, the first-order and the second-order multiscale numerical solutions given in (35)-(37), respectively. Here we take $M = 100$.

We compare the approximate solutions $\mathbf{E}^0_{M,h_0,h}(\mathbf{x}, t)$, $\mathbf{E}^{\varepsilon,1}_{M,h_0,h}(\mathbf{x}, t)$, $\mathbf{E}^{\varepsilon,2}_{M,h_0,h}(\mathbf{x}, t)$ with the numerical solution $\mathbf{E}^\varepsilon(\mathbf{x}, t)$ of the original problem (38) in a fine mesh. The numerical results are illustrated in Table 2 and Figs. 2 and 3. The numbers of elements and the degrees of freedoms are listed in Table 1.

TABLE 1. Comparison of computational effort in Example 5.1

	original equations	cell problem	homogenized equations
number of elements	93750	750	12000
number of dof	115075	1115	29860

TABLE 2. Comparison of the computational errors

	$\frac{\|\mathbf{e}_0\|_{(0)}}{\|\mathbf{E}^0_{M,h_0,h}\|_{(0)}}$	$\frac{\|\mathbf{e}_1\|_{(0)}}{\|\mathbf{E}^{\varepsilon,1}_{M,h_0,h}\|_{(0)}}$	$\frac{\|\mathbf{e}_2\|_{(0)}}{\|\mathbf{E}^{\varepsilon,2}_{M,h_0,h}\|_{(0)}}$	$\frac{\|\mathbf{e}_0\|_{(1)}}{\|\mathbf{E}^0_{M,h_0,h}\|_{(1)}}$	$\frac{\|\mathbf{e}_1\|_{(1)}}{\|\mathbf{E}^{\varepsilon,1}_{M,h_0,h}\|_{(1)}}$	$\frac{\|\mathbf{e}_2\|_{(1)}}{\|\mathbf{E}^{\varepsilon,2}_{M,h_0,h}\|_{(1)}}$
Case 5.1	0.95791	0.9565	0.3479	3.3374	3.1713	0.5733
Case 5.2	2.3747	2.3723	0.2618	12.5537	11.9917	0.5282
Case 5.3	2.2217	2.2216	0.4241	5.5493	5.1159	0.6535
Case 5.4	8.7191	8.7013	0.3718	23.4211	21.6238	0.6235

We introduce the notation: $\|\mathbf{u}\|_{(0)} = \|\mathbf{u}\|_{L^2(0,T;(L^2(\Omega))^3)}$, $\|\mathbf{u}\|_{(1)} = \|\mathbf{u}\|_{L^2(0,T;\mathbf{H}(\mathbf{curl};\Omega))}$,

$$\mathbf{e}_0(\mathbf{x},t) = \mathbf{E}^\varepsilon(\mathbf{x},t) - \mathbf{E}^0_{M,h_0,h}(\mathbf{x},t),$$
$$\mathbf{e}_1(\mathbf{x},t) = \mathbf{E}^\varepsilon(\mathbf{x},t) - \mathbf{E}^{\varepsilon,1}_{M,h_0,h}(\mathbf{x},t),$$
$$\mathbf{e}_2(\mathbf{x},t) = \mathbf{E}^\varepsilon(\mathbf{x},t) - \mathbf{E}^{\varepsilon,2}_{M,h_0,h}(\mathbf{x},t),$$

and

$$\text{error1} = \frac{\|\mathbf{e}_0\|_{(L^2(\Omega))^3}}{\|\mathbf{E}^0_{M,h_0,h}\|_{(L^2(\Omega))^3}}, \quad \text{error2} = \frac{\|\mathbf{e}_1\|_{(L^2(\Omega))^3}}{\|\mathbf{E}^{\varepsilon,1}_{M,h_0,h}\|_{(L^2(\Omega))^3}},$$
$$\text{error3} = \frac{\|\mathbf{e}_2\|_{(L^2(\Omega))^3}}{\|\mathbf{E}^{\varepsilon,2}_{M,h_0,h}\|_{(L^2(\Omega))^3}}, \quad \text{error4} = \frac{\|\mathbf{e}_0\|_{\mathbf{H}(\mathbf{curl};\Omega)}}{\|\mathbf{E}^0_{M,h_0,h}\|_{\mathbf{H}(\mathbf{curl};\Omega)}},$$
$$\text{error5} = \frac{\|\mathbf{e}_1\|_{\mathbf{H}(\mathbf{curl};\Omega)}}{\|\mathbf{E}^{\varepsilon,1}_{M,h_0,h}\|_{\mathbf{H}(\mathbf{curl};\Omega)}}, \quad \text{error6} = \frac{\|\mathbf{e}_2\|_{\mathbf{H}(\mathbf{curl};\Omega)}}{\|\mathbf{E}^{\varepsilon,2}_{M,h_0,h}\|_{\mathbf{H}(\mathbf{curl};\Omega)}}.$$

The relative numerical errors of the homogenization method, the first-order and the second-order asymptotic multiscale methods in the $L^2(0,t;(L^2(\Omega))^3)$-norm and in the
$L^2(0,t;\mathbf{H}(\mathbf{curl};\Omega))$-norm for Cases 5.1 and 5.2 are shown in Table 2.

Fig.2: (a)-(d) show the evolution of the relative errors for Cases 5.1 and 5.2 in $(L^2(\Omega))^3$-norm and in $\mathbf{H}(\mathbf{curl};\Omega)$-norm with respect to time t, $0 \le t \le 0.5$. The figures also reveal that the errors do not grow with time t, and this clearly demonstrates that our method is stable for long time simulations.

Fig.3 (a)-(h) show the numerical results for $\mathbf{E}^\varepsilon(\mathbf{x},t)$, $\mathbf{E}^{\varepsilon,1}_{M,h_0,h}(\mathbf{x},t)$, $\mathbf{E}^{\varepsilon,2}_{M,h_0,h}(\mathbf{x},t)$ and $\mathbf{E}^0_{M,h_0,h}(\mathbf{x},t)$ at time $T = 0.5$ at the intersection $x_3 = 0.5$ for Case 5.1, where $M = 100$.

Example 5.2 We consider problem (38), where a whole domain Ω and the reference cell Q are as shown in Fig.4: (a) and (b). There is an ellipsoid inclusion in Q, and the equation of the ellipsoid is given by

$$\frac{(\xi_1 - 0.5)^2}{0.16} + \frac{(\xi_2 - 0.5)^2}{0.16} + \frac{(\xi_3 - 0.5)^2}{0.16} = 1.$$

Two cases are considered in our numerical simulations. Let a_{ij1} denote the value of a_{ij} in the inside ellipsoid of Q and a_{ij0} be the value of a_{ij} in the other part of Q. The Kronecker symbol δ_{ij} and $\mathbf{a}^T$ are defined as in Example 5.1, and we set $\varepsilon = \frac{1}{3}$, $T = 0.8$.

Case 5.3: $a_{ij0} = 100\delta_{ij}$, $a_{ij1} = \delta_{ij}$; $\mathbf{f} = (500t, 500t, 500t)^T$.

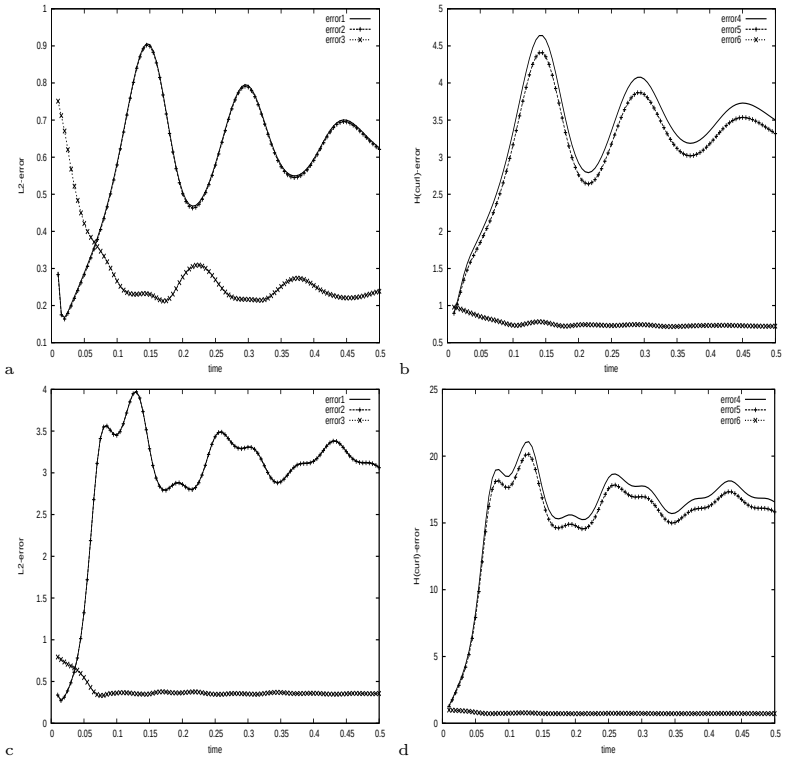

FIGURE 2. In Case 5.1: (a) the evolution of relative errors in the $(L^2(\Omega))^3$-norm; (b) the evolution of relative errors in the $\mathbf{H}(\mathbf{curl};\Omega)$-norm. In Case 5.2: (c) the evolution of relative errors in the $(L^2(\Omega))^3$-norm; (d) the evolution of relative errors in the $\mathbf{H}(\mathbf{curl};\Omega)$-norm.

TABLE 3. Comparison of computational effort in Example 5.2

	original equations	cell problem	homogenized equations
number of elements	253987	3542	48000
number of dof	298963	4319	59660

Case 5.4: $a_{ij0} = 1000\delta_{ij}$, $a_{ij1} = \delta_{ij}$; $\mathbf{f} = (5000t, 500t, 500t)^T$.

The numbers of the elements and the degrees of freedoms are listed in Table 3. We take the time step $\Delta t = 0.005$.

The relative numerical errors of the homogenization method, the first-order and the second-order asymptotic multiscale methods in the $L^2(0,t;(L^2(\Omega))^3)$-norm and in the
$L^2(0,t;\mathbf{H}(\mathbf{curl};\Omega))$-norm for Cases 5.3 and 5.4 are listed in Table 2. The evolution of the relative errors for Cases 5.3 and 5.4 in the $L^2(0,t;(L^2(\Omega))^3)$-norm and in the $L^2(0,t;\mathbf{H}(\mathbf{curl};\Omega))$-norm are illustrated in Fig.5.

In Fig.6:(a)-(h), the numerical results for solutions $\mathbf{E}^\varepsilon(\mathbf{x},t)$, $\mathbf{E}^{\varepsilon,1}_{M,h_0,h}(\mathbf{x},t)$, $\mathbf{E}^{\varepsilon,2}_{M,h_0,h}(\mathbf{x},t)$,$\mathrm{E}^0_{M,h_0,h}(\mathbf{x},t)$ at time $T = 0.5$ at the intersection $x_3 = 0.5$ for Case 5.3, where $M = 100$.

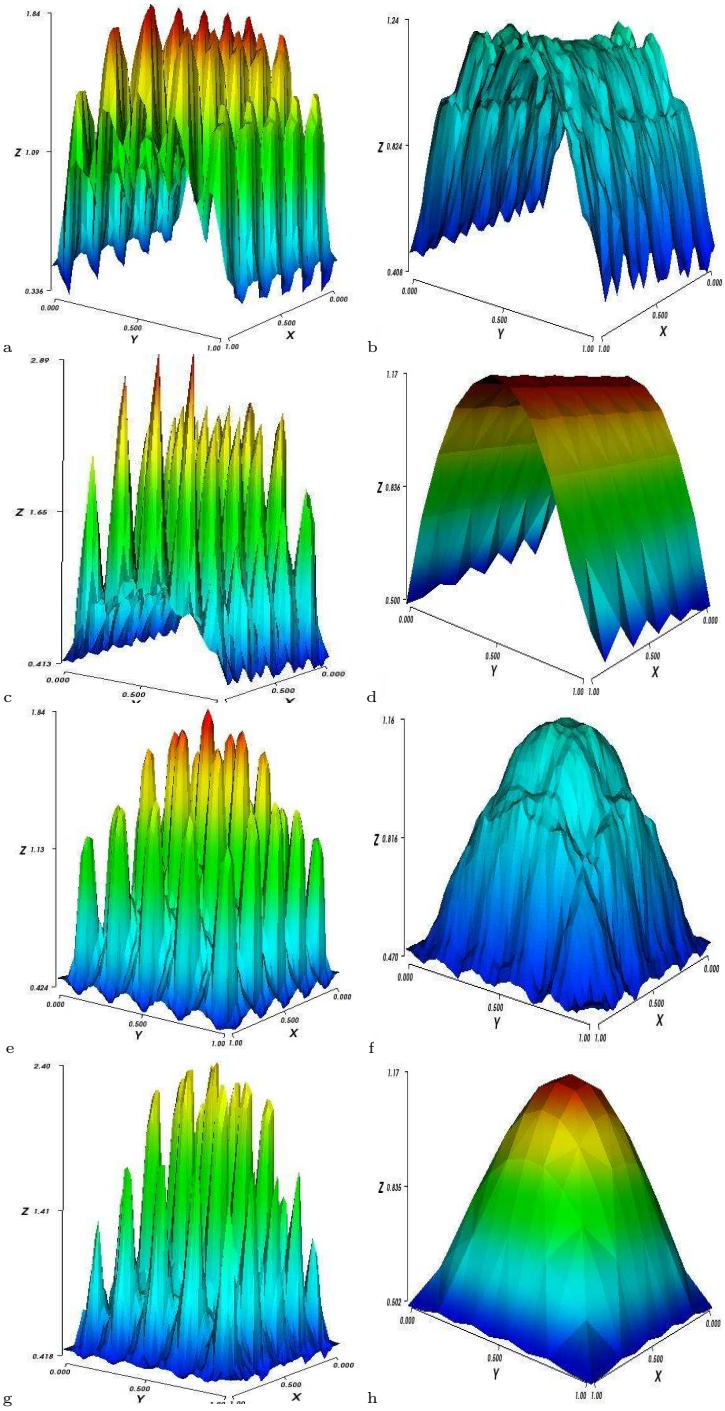

FIGURE 3. In Case 5.1: (a) The first component of the solution $\mathbf{E}^{\varepsilon}$ in a fine mesh; (b)the first component of the first-order multiscale numerical solution $\mathbf{E}^{\varepsilon,1}_{M,h_0,h}$; (c)the first component of the second-order multiscale numerical solution $\mathbf{E}^{\varepsilon,2}_{M,h_0,h}$; (d)the first component of the homogenized solution $\mathbf{E}^{0}_{M,h_0,h}$ in a coarse mesh. In Case 5.1: (e) The third component of the solution $\mathbf{E}^{\varepsilon}$ in a fine mesh; (f)the third component of the first-order multiscale numerical solution $\mathbf{E}^{\varepsilon,1}_{M,h_0,h}$; (g)the third component of the second-order multiscale numerical solution $\mathbf{E}^{\varepsilon,2}_{M,h_0,h}$; (h)the third component of the homogenized solution $\mathbf{E}^{0}_{M,h_0,h}$ in a coarse mesh.

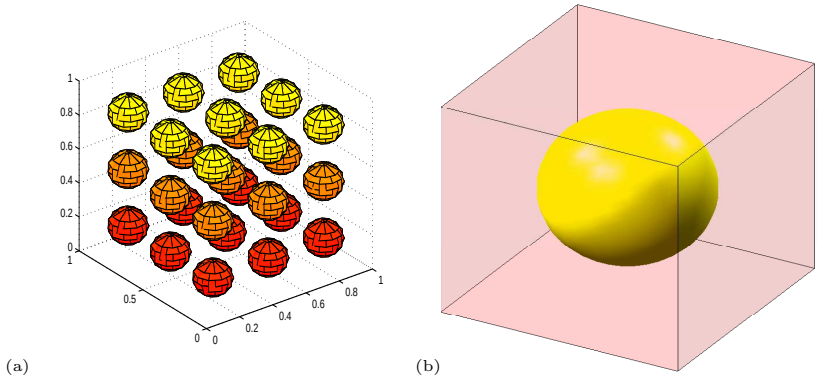

FIGURE 4. (a) Domain Ω; (b) the reference cell Q.

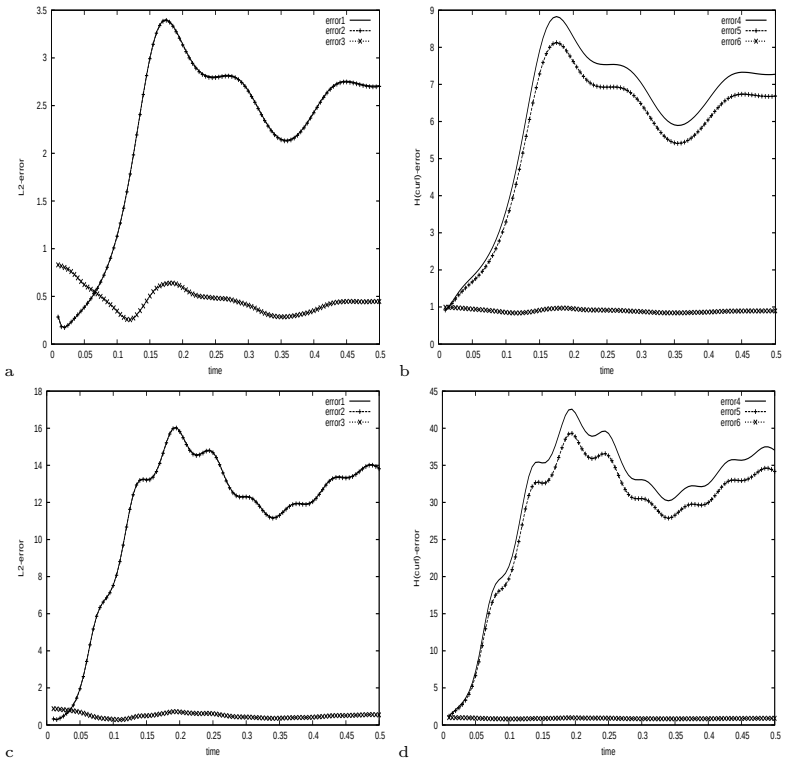

FIGURE 5. In Case 5.3: (e) the evolution of relative errors in the $(L^2(\Omega))^3$-norm; (f) the evolution of relative errors in the $\mathbf{H}(\mathbf{curl};\Omega)$-norm. In Case 5.4: (a) the evolution of relative errors in the $(L^2(\Omega))^3$-norm; (b) the evolution of relative errors in the $\mathbf{H}(\mathbf{curl};\Omega)$-norm;

Remark 5.1 From the results presented in Table 2 and Figs.2-3 and 5-6, we observe that when the difference between various materials is large, the homogenization method and the first-order multiscale method fail to provide satisfactory

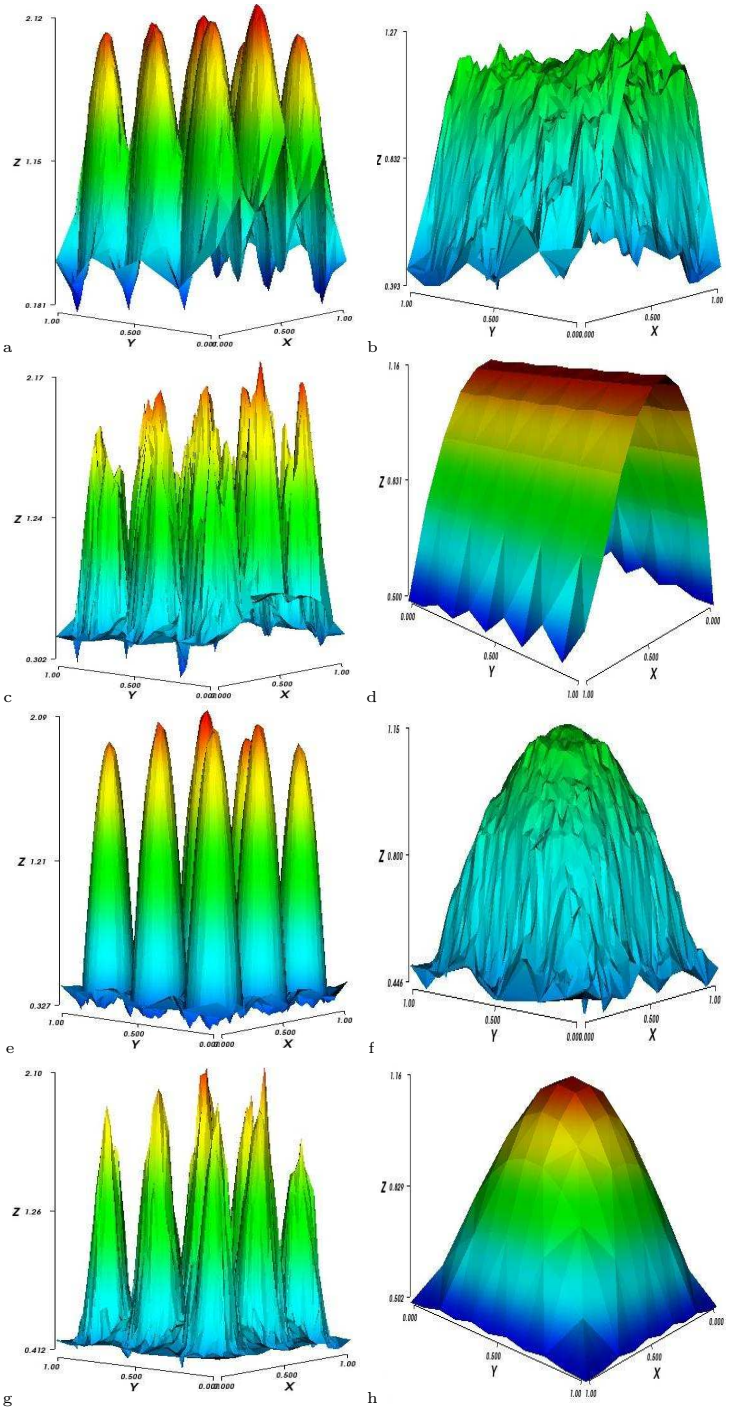

FIGURE 6. In Case 5.3: (a) The second component of the solution $\mathbf{E}^{\varepsilon}$ in a fine mesh; (b)the second component of the first-order multiscale numerical solution $\mathbf{E}^{\varepsilon,1}_{M,h_0,h}$; (c)the second component of the second-order multiscale numerical solution $\mathbf{E}^{\varepsilon,2}_{M,h_0,h}$; (d) the second component of the homogenized solution $\mathbf{E}^{0}_{M,h_0,h}$ in a coarse mesh. In Case 5.3: (e) The third component of the solution $\mathbf{E}^{\varepsilon}$ in a fine mesh; (f)the third component of the first-order multiscale numerical solution $\mathbf{E}^{\varepsilon,1}_{M,h_0,h}$; (g)the third component of the second-order multiscale numerical solution $\mathbf{E}^{\varepsilon,2}_{M,h_0,h}$; (h)the third component of the homogenized solution $\mathbf{E}^{0}_{M,h_0,h}$ in a coarse mesh.

results. The second-order multiscale approach is clearly the best among the computation schemes studied in this paper.

Conclusions In this paper, we discussed the multiscale method for the time-dependent Maxwell's equations with memory effects in composite materials. Numerical simulations were carried out to validate the multiscale numerical algorithm in the present paper. It should be emphasized that our method has two advantages: First, we can present the multiscale approach for the time-dependent Maxwell's equations with memory effects. Second, we can solve a finite set of stationary Maxwell's equations on separate processors. In contrast, the normal step-by-step time-marching methods for the evolution equations are not easily parallelizable.

References

[1] R. Beck, R. Hiptmair, R.H.W. Hoppe and B. Wohlmuth, Residual based on *a posteriori* estimates for eddy current computation, *M2AN Math. Model. Numer. Anal.*(2000), 34: 159-182.

[2] A. Bensoussan, J.L. Lions and G. Papanicolaou, *Asymptotic Analysis for Periodic Structures*, North-Holland, Amsterdam, 1978.

[3] A. Bossavit, G. Griso and B. Miara, Modelling of periodic electromagnetic structures bianisotropic materials with memory effects, *Journal of Mathématiques Pures et Appliqués,*(2005), 84: 819-850.

[4] L.Q. Cao, Y. Zhang, W. Allegretto and Y.P. Lin, Multiscale asymptotic method for the Maxwell's equations in composite materials, *SIAM J. Numer. Anal.*(2010) 47(6): 4257-4289.

[5] Y. Zhang, L.Q. Cao and Y.S. Wong, Multiscale computations for 3D time-dependent Maxwell's equations in composite materials,*SIAM J. Sci. Comput.*(2010) 32(5): 2560-2583.

[6] C.M. Chen and T.M. Shih, *Finite elements methods for integro-differential equations*, World Scientific Pub. Co., Singapore, 1998.

[7] Z. Chen, L. Wang and W. Zheng, An adaptive multilevel method for time-harmonic Maxwell equations with sigularities, *SIAM J. Sci. Comput.*(2007), 29: 118-138.

[8] M. Costabel, M. Dauge and S. Nicaise, Sigularities of Maxwell interface problems, *M2AN Math. Model Numer. Anal.*(1999), 33: 627-649.

[9] M. Costabel, M. Dauge, Singularities of electromagnetic fields in polyhedral domains, *Arch. Rational Mech. Anal.*(2000), 151: 221-276.

[10] G. Duvaut and J.L. Lions, *Inequalities in Mechanics and Physics*, Springer-Verlag, 1976.

[11] M. El Feddi, Z. Ren, A. Razek, A. Bossavit, Homogenization technique for maxwell equations in periodic structures, *IEEE Trans.on Magnetics*(1997), 33: 1382-1385.

[12] V. Girault and P.A. Raviant, *Finite Element Methods for Navier-Stokes equations,* Springer-Verlag, 1986.

[13] V.V. Jikov, S.M. Kozlov, O.A. Oleinik, *Homogenization of Differential Operators and Integral Funtionals,* Spinger-Verlag, 1994.

[14] W. McLean, I.H. Sloan and V. Thomée, Time discretization via laplace transformation of an integro-differential equation of parabolic type, *Numer. Math.*(2006), 102: 497-522.

[15] W. McLean and V. Thomée, Time discretization of an evolution equation with laplace transforms, *IMA J. Numer. Anal.*(2004), 24: 439-463.

[16] P. Monk, *Finite Element Methods for Maxwell's Equations* , Clarendon press, Oxford, 2003.

[17] J. Nédélec, Mixed finite elements in R^3, *Numer.Math.*(1980), 35: 315-341.

[18] J. Nédélec, A new family of Mixed finite elements in R^3, *Numer.Math.*(1986), 50: 57-81.

[19] O.A. Oleinik, A.S. Shamaev and G.A. Yosifian, *Mathematical Problems in Elasticity and Homogenization* , North-Holland, Amsterdam, 1992.

[20] E. Sanchez-Palencia, *Non-Homogeneous Media and Vibration Theory*, Springer-Verlag Berlin Heidelberg New York, 1980.

[21] D.W. Sheen, I.H.Sloan and V.Thomée, A parallel method for time discretization of parabolic equations based on laplace transformation and quadrature, *IMA Journal of Numerical Analysis*(2003), 23: 269-299.

[22] D.Y. Tzou, *Macro-to Microscale heat transfer, the lagging behavior*, Washing: Taylor Francis publishers, 1997.

[23] N. Wellander, Homogenization of the Maxwell equations: Case I. Linear Theory, *Appliactions of Mathematics*(2001), 46:29-51.

[24] N. Wellander, Homogenization of the Maxwell equations: Case II. Nonlinear Conductivity, *Appliactions of Mathematics*(2002), 47: 255-283.
[25] N. Wellander and G. Kristensson, Homogenization of the Maxwell equations at fixed frequency,*SIAM J.Appl.Math.* (2003), 64(1): 170-195.
[26] F.M. Zhai, *Multiscale Modeling and Algorithm for Heat Transfer Problem of Composite Materials*, Ph.D thesis, Chinese Academy of Sciences, 2009.

Institute of Computational Mathematics and Scientific/Engineering Computing, Academy of Mathematics and Systems Science, Chinese Academy of Sciences, Beijing, 100190, China
E-mail: zhangya@lsec.cc.ac.cn

LSEC, Institute of Computational Mathematics and Scientific/Engineering Computing, Academy of Mathematics and Systems Science, Chinese Academy of Sciences, Beijing, 100190, China
E-mail: clq@lsec.cc.ac.cn

Department of Mathematical and Statistical Sciences, University of Alberta, Edmonton, Alberta T6G 2G1, Canada
E-mail: wallegre@math.ualberta.ca

Department of Applied Mathematics, Room HJ 631, Stanley Ho Building, The Hong Kong Polytechnic University, Hung Hom, Kowloon, Hong Kong, China and Department of Mathematical and Statistical Sciences, University of Alberta, Edmonton, Alberta T6G 2G1, Canada
E-mail: ylin@math.ualberta.ca; malin@polyu.edu.hk